Available online at www.sciencedirect.com

ScienceDirect

Acta Materialia 81 (2014) 248–257

Acta MATERIALIA

www.elsevier.com/locate/actamat

Strain-controlled cyclic stability and properties of Cu with highly oriented nanoscale twins

Q.S. Pan, L. Lu *

Shenyang National Laboratory for Materials Science, Institute of Metal Research, Chinese Academy of Sciences, Shenyang 110016, People's Republic of China

Received 5 May 2014; received in revised form 21 July 2014; accepted 4 August 2014

Abstract

By means of a direct-current electrodeposition technique, bulk (~3 mm in thickness) polycrystalline Cu samples with preferentially oriented nanoscale twins have been synthesized. Strain-controlled pull–push fatigue tests of the nanotwinned Cu samples show that the cyclic stability is maintained after a short initially rapid cyclic hardening stage, distinct from continuous cyclic softening of ultrafine-grained Cu. The saturation stress increases with increasing strain amplitude and decreasing twin thickness, while the longer low cycle fatigue life is achieved at larger grain size. The strain–life and *S–N* curves reveal that the preferentially oriented nanotwins embedded in microsized grains enhance the low and high cycle fatigue property synergy for nanotwinned Cu, which has better low cycle fatigue life while maintaining higher endurance limit (90 MPa at 10^7), compared with that of coarse-grained Cu and ultrafine-grained Cu. Besides the relatively stable microstructure, the activation of a single primary slip system, i.e. threading dislocation propagation inside nanoscale twin lamellar channels, dominates the steady state of nanotwinned samples.

Keywords: Nanoscale twins; Strain-controlled fatigue; Cu; Cyclic stability; Fatigue property

1. Introduction

Recently, engineering coherent twin boundaries (TBs) at the nanoscale has been regarded as an effective approach for achieving high strength while maintaining substantial work hardening ability and considerable ductility [1–5]. On the one hand, coherent TBs act as effective barriers for the motion of dislocations, resulting in significant TB strengthening, analogous to that induced by grain boundary (GB) strengthening [3–5]. On the other hand, a high density of coherent TBs can provide enough room for dislocation accumulation and storage, which is fundamentally different from the conventional incoherent GBs [2–5].

Uniaxial mechanical properties and deformation mechanism for nanotwinned materials have been extensively studied by experimental tests [2–4,6–8], crystal plasticity modeling [5,9] and molecular dynamics simulations [10–13]. Fatigue properties of nanotwinned Cu (nt-Cu) samples in the high-cycle fatigue (HCF) regime were also investigated under tension–tension stress-controlled fatigue tests [14–18]. Shute et al. [15,16] investigated the magnetron sputtered Cu foils with highly oriented nanotwins (sample thickness ~ 170 μm) by tension–tension stress-controlled cycling. The *S–N* curve shows that the fatigue life and fatigue limit (at the fatigue life of 10^7 cycles) of nt-Cu are enhanced over that of coarse-grained (CG-) Cu. Although the majority of nanotwinned structures are quite stable, numerous TBs are destroyed. Instead, many dislocation walls are formed, especially at the intersection between nanotwinned columns and adjacent detwinned columns.

* Corresponding author. Tel.: +86 24 23971939; fax: +86 24 23998660.
E-mail address: llu@imr.ac.cn (L. Lu).

http://dx.doi.org/10.1016/j.actamat.2014.08.011
1359-6454/

The soft detwinned regions result in the surface depression appearance and cause the surface crack initiation [16].

Polycrystalline columnar-grained Cu samples with preferentially oriented nanotwins in larger grain size were also subjected to tension–tension stress-controlled fatigue tests [18]. Due to the presence of a high density of preferentially oriented nanotwins, the fatigue life of nt-Cu in the *S–N* curve is significantly enhanced. Microstructural observations demonstrate that most TBs are quite stable under cyclic deformation. The fatigue behavior of the polycrystalline nt-Cu samples resembles that in a "quasi-single" crystal metal, where only one primary slip system, i.e. the threading dislocation, is preferentially activated and dominates the cyclic deformation of nt-Cu when the cyclic loading axis is parallel to the twin plane. Schmid factor analysis demonstrates that propagation of such uniform threading dislocations within nanoscale twin channels gives rise to the "zigzag" slip bands across a few TBs. The effective confinement of threading dislocations within nanotwin lamellae and smaller slip bands retard fatigue crack initiation, thereby contributing to an enhanced fatigue limit and fatigue life of nt-Cu.

In terms of intensively studying the fatigue performance and cyclic deformation mechanism of nt-Cu, high cyclic fatigue tests with stress control are clearly insufficient [19]. Classical approaches to fatigue design involve the characterization of total fatigue life to failure in terms of the cyclic stress range (the *S–N* curve approach) or the (plastic or total) strain range [19]. Under high-cycle, low-stress fatigue situations, the materials deform primarily elastically; the failure time or the number of cycles to failure under such HCF regime has traditionally been characterized in terms of the strength. However, the stresses associated with low-cycle fatigue (LCF) are generally high enough to cause appreciable plastic deformation prior to failure, which is closely correlated with its ductility. Therefore, under this circumstance, the fatigue life is characterized in terms of its strain.

Clearly, the different approaches of the stress-controlled and strain-controlled fatigue tests provide apparently different guidelines for evaluating the properties of metallic materials, especially for high-strength metals with limited plastic ductility, like the ultrafine-grained (UFG) and nanocrystalline (NG) metals, which usually exhibit high strength but very limited tensile ductility. The stress-controlled fatigue life and endurance limit of high-strength UFG and NG metals are much elevated in the HCF regime compared to their conventional CG counterparts [20–26]. Unfortunately, in the LCF regime, UFG and NG materials exhibit a much shorter fatigue life (several times smaller) than that of CG counterparts under strain-controlled conditions, due to a lack of ductility [27–35]. Moreover, the continuous cyclic softening phenomenon is prevalently observed in UFG and NG materials fatigued in strain-controlled tests [22,29].

Meanwhile, the nanolamellar metallic materials also contribute a sustainable high strength due to confinement of slip between nanoscale interfaces and very limited uniform ductility [36,37]. A relatively longer fatigue life and higher endurance limit of nanolaminated materials had been observed in the HCF regime [38–41]. However, it could be predicted that the fatigue properties of nanolamellar metals in the LCF regime may not be as desirable as in the HCF regime if the strain-controlled fatigue tests could be performed on the sample with a large enough sample size.

Therefore, the LCF tests under strain control can be used to accurately explore the ductility and fatigue mechanisms of nanostructured metals. However, due to the limitations of sample preparation, most nanostructured metals have a very limited sample thickness, typically in a range of tens to hundreds of micrometers. The limited thickness makes both strain-controlled LCF tests and compression tests very difficult (or impossible) because the strain gauge extensometer cannot be clamped onto the specimen surface. To date, fully reversed tension–compression fatigue tests on nanotwinned materials under strain and stress control have not been carried out, mainly owing to the limitation of the sample thickness. It is thus still uncertain whether the cyclic stress response of nt-Cu is cyclic hardening or softening under strain control, or whether nanotwins could improve the fatigue life in the LCF regime under strain control or not.

In this study, real bulk (~3 mm in thickness) polycrystalline Cu samples with preferentially oriented nanoscale twins have been synthesized by means of a direct-current electrodeposition. Fully reversed tension–compression fatigue tests were performed on the bulk Cu samples containing preferentially oriented nanoscale twins under constant strain-controlled and stress-controlled fatigue tests, respectively. The fatigue properties, including information about the cyclic stress/strain response, the fatigue life in the LCF regime and the fatigue limit in the HCF regime, were explored and the underlying cyclic stress/strain response associated with the effect of microstructure features, including TB orientation, twin thickness and twin lamellar length (i.e. grain size), discussed.

2. Experimental

Bulk high-purity copper sheets containing preferentially oriented nanoscale growth twins were synthesized by means of direct-current electrodeposition in an electrolyte of $CuSO_4$. The substrate was a pure Ti sheet. The final thickness of the nt-Cu plates was ~3.4 mm. By controlling the current densities (20 and 30 mA cm^{-2}, respectively), two pieces of nt-Cu samples with different grain sizes and twin thicknesses (named nt-Cu-A and nt-Cu-B, respectively) were obtained. For comparison, high-purity twin-free UFG-Cu samples were produced by cold-rolling CG-Cu samples with a rolling strain, $\varepsilon = (t_0 - t)/t = 400\%$ (where t_0 and t denote the thickness of the initial and the as-rolled samples, respectively). After annealing UFG-Cu samples at 250 °C for 2 h in air, CG-Cu samples having a

grain size analogous to that of nt-Cu were also produced. The other details of the sample preparation procedures are described in Ref. [18].

Dog-bone-shaped specimens were cut from nt-, UFG- and CG-Cu sheets with a gauge cross-section area of $4 \times 3\ mm^2$ and a length of 12 mm using an electrical spark machine. All specimens were mechanically ground to the desired dimensions, followed by the electropolishing to minimize the surface roughness and obtain a strain-free surface.

Uniaxial symmetrical tension–compression tests were performed on an Instron 8874 testing machine under constant strain and stress control at room temperature in air. The cyclic loading axis was approximately parallel to most of the twin planes. Under the strain control, a dynamic strain gauge extensometer (Instron Catalogue No. 2620-603) with a gauge length of 10 mm was clamped onto the specimen surface by a high-strength rubber band for accurate direct measurement and the closed-loop control of strain in the materials undergoing cyclic testing. The strain resolution and control precision are less than 10^{-4}. The applied uniaxial plastic strain amplitudes ranged from 2.0×10^{-4} to 3.16×10^{-3} and the uniaxial total strain amplitudes ranged from 3.16×10^{-4} to 5.6×10^{-3}. Under strain control, a triangular wave was used and the cyclic strain rate was 2.5×10^{-3}. The fatigue process was stopped when the cyclic stress amplitude dropped by 70% relative to the largest stress amplitude. For comparison, the cyclic deformed nt-Cu samples were interrupted at 50 cycles at the uniaxial plastic strain amplitude of 3.16×10^{-3}. In the stress-controlled fatigue tests, a sinusoidal wave was used and the applied frequency was 30 Hz. The fatigue limit of nt-Cu was tested by the staircase method strictly [18,19].

The plane view and cross-section microstructures of the nt-Cu specimens before and after fatigue were characterized by field emission gun scanning electron microscopy (SEM) in a FEI Nova NanoSEM 430 with backscattered electron imaging using a VCD detector. The cross-section microstructures of Cu specimens before and after fatigue were also studied by a FEI Tecnai F20 transmission electron microscope (TEM) operated at 200 kV. The TEM Cu foils were thinned by twin-jet polishing in an electrolyte of phosphoric acid (25%), alcohol (25%) and deionized water (50%) at about −10 °C.

3. Results

3.1. As-deposited nt-Cu

The overall 3-D microstructures of the nt-Cu samples are illustrated in Ref. [18]. The polycrystalline grains of nt-Cu are columnar in shape and are subdivided by parallel twin lamellae, with most TBs parallel to the deposition plane. Fig. 1 shows the distributions of grain size and twin thickness for the nt-Cu-A and nt-Cu-B samples. The grain sizes of both samples have a wide distribution, from 1 to 20 μm. The average grain sizes for nt-Cu-A and -B are ~4.6 and ~6.7 μm, respectively. The twin thickness exhibits a broad distribution from several nanometers to ~500 nm, but most of them are on the nanometer scale. The average twin thickness (λ) is ~54 nm for nt-Cu-A and ~75 nm for nt-Cu-B. All of the detailed information for the two nt-Cu samples is summarized in Table 1. The electron backscatter diffraction analysis indicates that both nt-Cu-A and -B have a strong {1 1 1} out-of-plane texture. The microstructure of the nt-Cu samples in this study is similar to that of the nt-Cu samples in Refs. [15,16]. However, the grain sizes of the present nt-Cu specimens are much larger than those (~500 nm) of the nt-Cu samples in Ref. [15].

It should be emphasized that the microstructure of the nt-Cu samples along the deposition direction is relatively homogeneous, as verified by microstructural observations. For cold-rolled UFG-Cu, most ultrafine grains are elongated, with an aspect ratio of ~2.4. The average transverse grain size is ~0.38 μm and the longitudinal grain size is ~0.92 μm, respectively, as shown in Table 1. The grain size of CG-Cu obtained by annealing UFG-Cu is ~9.8 μm, which is somewhat larger than that of nt-Cu-B and twice that of nt-Cu-A.

3.2. Strain-controlled fatigue properties of nt-Cu

3.2.1. Cyclic hardening and saturation

The cyclic stress response ($\Delta\sigma/2$) of the nt-Cu samples fatigued under different constant plastic strain amplitudes is shown in Fig. 2. Obviously, cyclic stability is maintained in nt-Cu samples after initially rapid hardening in a few cycles (~50). This phenomenon is fundamentally distinct from continuous cyclic softening of UFG-Cu under strain control [22,29]. For comparison, the stress amplitude of cold-rolled UFG-Cu samples fatigued at $\Delta\varepsilon_{pl}/2 = 1.78 \times 10^{-3}$ drops from ~375 MPa at the first cycle to ~273 MPa at the 100th cycle. In contrast, for CG-Cu with a grain size of ~9.8 μm, continuous cyclic hardening is observed throughout the whole fatigue life at large plastic strain amplitudes. The following general trends for fatigued nt-Cu in Fig. 2 should be noted:

The saturation stress of nt-Cu samples is dependent on the twin thickness. The smaller the twin thickness, the higher the saturation stress, consistent with the twin thickness dependence of yield strength (σ_y) and ultimate tensile strength (σ_{uts}) for nt-Cu in tensile tests [6]. The saturation stress amplitude ($\Delta\sigma/2$) of nt-Cu-A at $\Delta\varepsilon_{pl}/2 = 1.89 \times 10^{-3}$ is 402 MPa, which is much larger than that (294 MPa) of nt-Cu-B at $\Delta\varepsilon_{pl}/2 = 1.78 \times 10^{-3}$. Enhanced fatigue life is obtained in nt-Cu samples with increasing grain size. As shown in Fig. 2, the fatigue life of nt-Cu-B is comparable to that of its CG-Cu counterpart and generally longer than that of nt-Cu-A at a given strain amplitude.

The fully reversed tension–compression strain-controlled fatigue tests of nt-Cu samples demonstrated an obvious cyclic stability and improved fatigue life in the

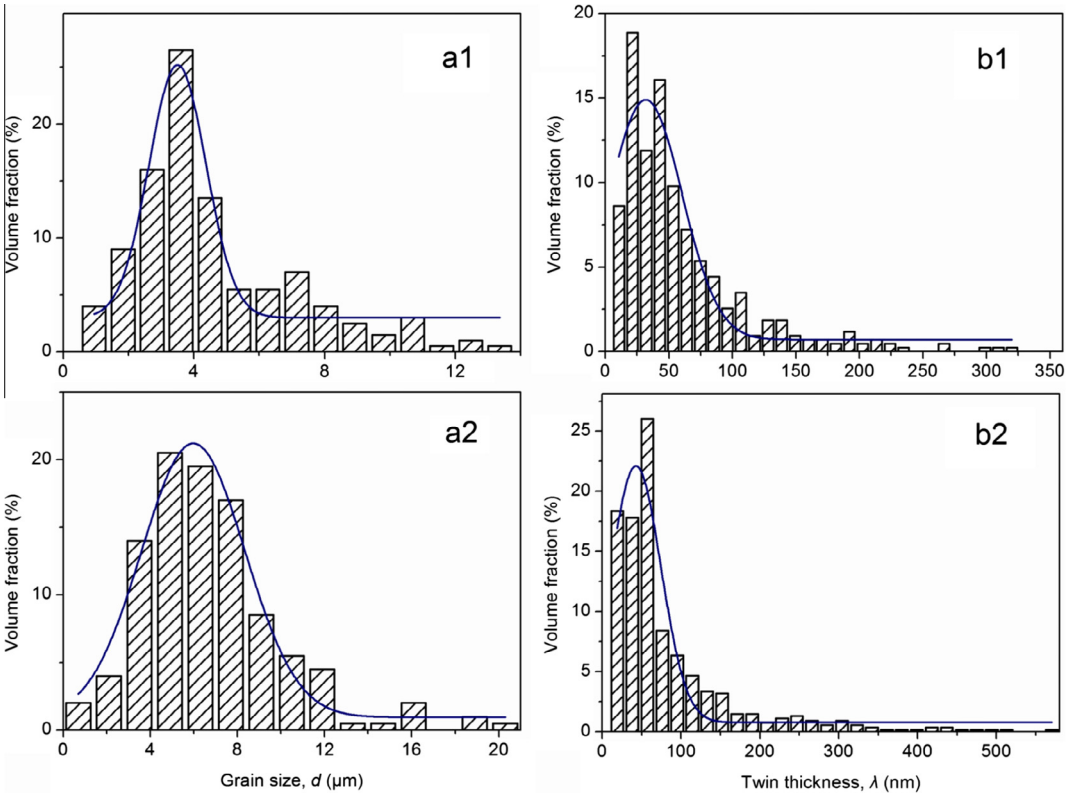

Fig. 1. The distributions of grain size (a1, a2) and twin thickness (b1, b2) of nt-Cu-A and nt-Cu-B samples.

Table 1
Summary of the microstructural characteristics of nt-Cu, CG-Cu and UFG-Cu samples.

Sample	d (μm)	λ (nm)
nt-Cu-A	4.6 ± 2.5	54 ± 50
nt-Cu-B	6.7 ± 3.3	75 ± 85
CG-Cu	9.8 ± 5.5	–
UFG-Cu	$d_T = 0.38 \pm 0.35$	
	$d_L = 0.92 \pm 1.57$	–

d is the average grain size; λ is the average twin thickness; d_T and d_L denote the grain size along the transverse and longitudinal directions of UFG-Cu, respectively.

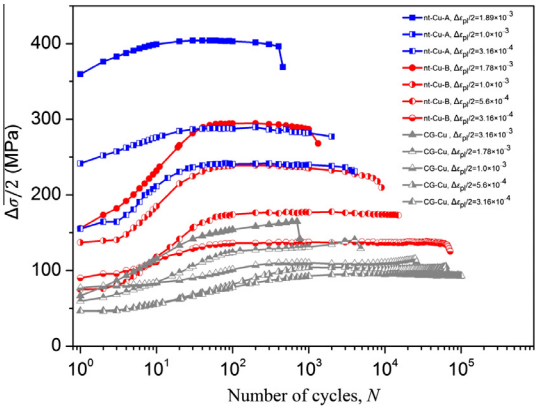

Fig. 2. Cyclic stress response ($\Delta\sigma/2$) of nt-Cu-A, nt-Cu-B and CG-Cu samples fatigued at different constant plastic strain amplitudes ($\Delta\varepsilon_{pl}$) vs. number of cycles (N).

LCF regime. The cyclic deformed nt-Cu samples reach the set value of the imposed plastic strain amplitude quickly, within ~30 cycles. For the nt-Cu-B samples, the typical evolution of the hysteresis loops at $\Delta\varepsilon_{pl}/2 = 1.78 \times 10^{-3}$ is shown in Fig. 3a. For the first few cycles, the stress amplitude increases with increasing plastic strain amplitude. Even when fatigued at a constant plastic strain amplitude in the next few cycles (~20), cyclic hardening of nt-Cu-B is still noticeable in Figs. 2 and 3. With continued cyclic straining, the rate of hardening progressively diminishes and a quasi-steady state of cyclic deformation, known as "cyclic saturation/stability", is reached. Once saturation is achieved, the stress amplitude is almost unaltered by further cycling, and the stress–strain hysteresis loop reaches a stable configuration as well. As seen in Fig. 3a, the steady-state hysteresis loops for the following different cycles nearly overlap with each other. Note that the stress amplitudes in compression are a few percent (<7%) larger than those in tension for nt-Cu samples (Fig. 3).

A series of hysteresis loops of nt-Cu in saturation, i.e. corresponding to a fixed 100th cycle, are summarized in Fig. 3b. It can be seen that the applied plastic strain amplitude plays a crucial role in the saturation stress of nt-Cu samples. The larger the strain amplitude applied, the higher the saturation stress achieved. Nonetheless, the shapes of the hysteresis loops for nt-Cu in saturation are slim and pointed, almost independent of the imposed plastic strain amplitude. Also, for nt-Cu samples, a small percentage of the plastic strain ($\varepsilon_{res}/2$) is reversed during unloading.

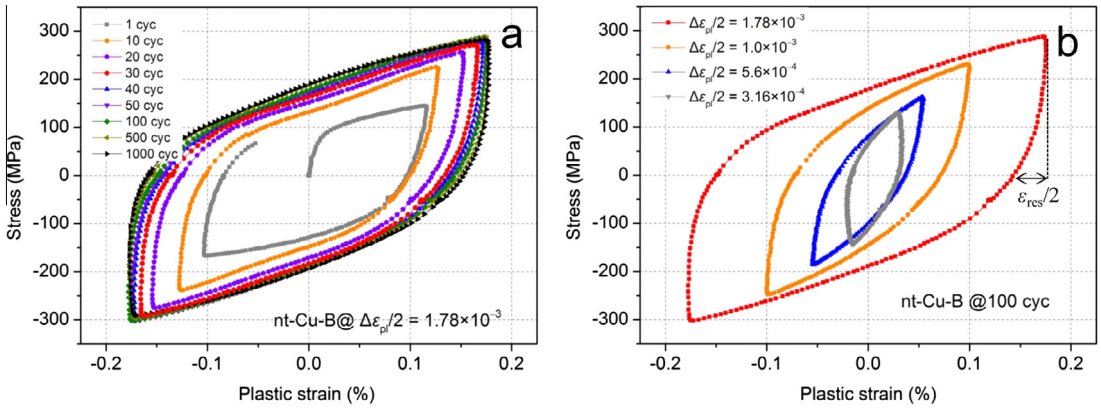

Fig. 3. (a) Development of the hysteresis loops of nt-Cu-B samples fatigued at $\Delta\varepsilon_{pl}/2 = 1.78 \times 10^{-3}$. (b) Changes of steady-state hysteresis loop of nt-Cu-B samples fatigued at different constant plastic strain amplitudes.

3.2.2. Cyclic stress–strain curve

The cyclic stress–strain curves, obtained by plotting the saturation shear stress (τ_s) as a function of the plastic resolved shear strain amplitude (γ_{pl}) for nt-Cu samples, are displayed in Fig. 4. For comparison, the data for single crystal [42,43] and CG Cu in this study are also included. The relationship between the resolved shear stress/plastic strain amplitude and the uniaxial stress/plastic strain amplitude is as follows [19]:

$$\tau_s = m\Delta\sigma/2$$
$$\gamma_{pl} = \Delta\varepsilon_{pl}/(2m) \quad (1)$$

where m is the Schmid factor for the single-crystal Cu or the Sachs/Taylor factor for polycrystalline Cu. The m value is 0.5 for the single-crystal Cu with single-slip orientation; it is 0.45 for single-slip-oriented CG-Cu based on the Sachs model and 0.33 for multiple-slip-oriented CG-Cu following the Taylor model.

As illustrated in Ref. [18], the fatigue behavior of polycrystalline nt-Cu samples resembles that in a fatigued "quasi-single" crystal metal, where there is only one primary slip system with the slip direction parallel to the TBs, but the slip plane inclined to the TBs is preferentially activated when the cyclic loading axis is parallel to twin planes. The dislocations belonging to this slip system are like the threading dislocations observed in nanoscale thin films and multilayer materials [44]. Schmid factor calculations reveal that the maximum m for the threading dislocation is ~0.47 in a few grains with specific in-plane orientations, where its Burgers vector is at 45° relative to the loading axis. This is consistent with slip band traces on the top surface at ~45° relative to the loading axis observed in some cyclically plastic deformed grains, as shown in Fig. 4 in Ref. [18].

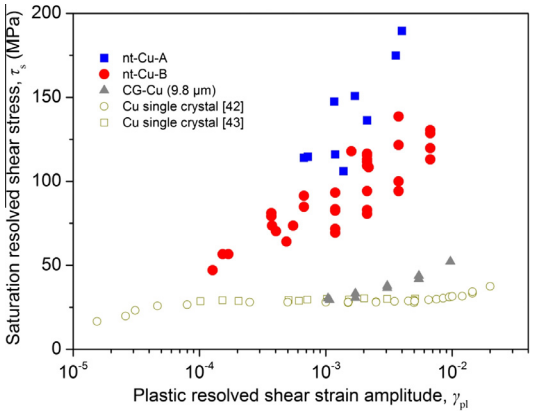

Fig. 4. Cyclic stress–strain curves of nt-Cu-A, nt-Cu-B and CG-Cu samples. Data for single-crystal Cu with a single slip system [42,43] are included for comparison.

Apparently, due to the presence of a high density of nanoscale twins, the saturation shear stresses for nt-Cu are much larger than those of CG-Cu and single-crystal Cu. Furthermore, nt-Cu-A samples with smaller average twin thickness have larger saturation shear stresses than nt-Cu-B at the same plastic resolved shear strain amplitude. Unlike the plateau regime for single-crystal Cu, the cyclic stress–strain curves for nt-Cu samples exhibit a continuous increase in the saturation stress with increasing plastic strain amplitude, as shown in Fig. 4. This suggests that nanoscale twins embedded in microsized grains play an important role in the cyclic deformation of nt-Cu.

4. Discussion

4.1. Cyclic stability mechanism and twin thickness dependence of saturation stress

The cyclic stress–strain response of single crystal and CG Cu associated with cyclic deformation mechanisms have been well studied by experiments [42,43,45–53] and modeling [54]. It is accepted that the cyclic saturation behavior is prevalently observed in single-crystal Cu with single-slip orientation [51–53] and CG-Cu with a large grain size [33,45–49]. The cyclic steady deformation suggests that the dislocation density remains constant in the single slip-induced dislocation patterns, such as veins composed of dense dislocation dipole arrays at very small γ_{pl} ($<6 \times 10^{-5}$) and persistent slip bands (PSBs) with

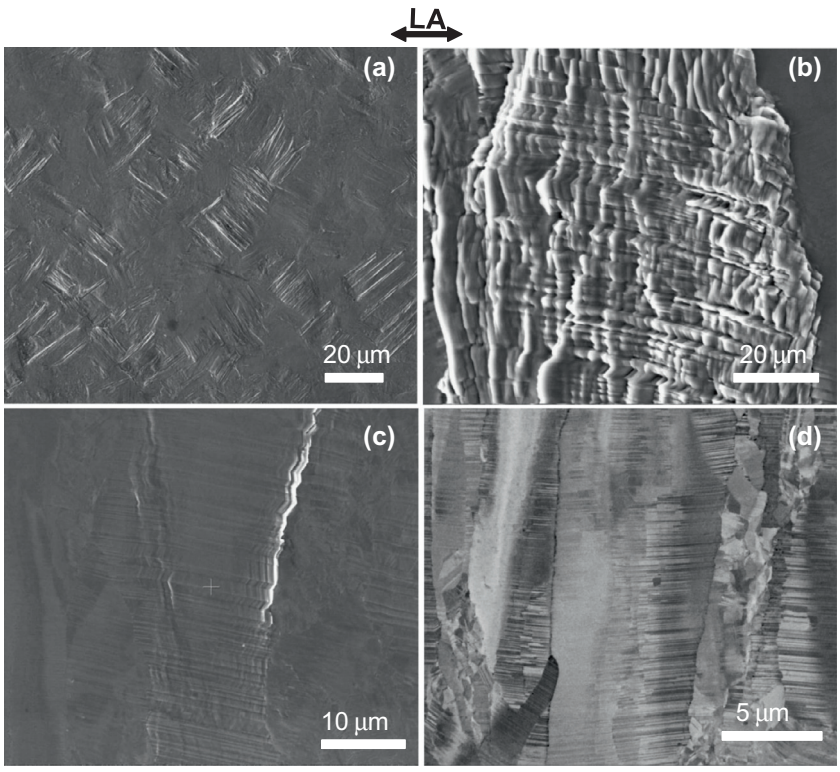

Fig. 5. Typical SEM images of nt-Cu-B samples in plane view (a) and cross-section view (b) fatigued at $\Delta\varepsilon_{pl}/2 = 1.78 \times 10^{-3}$ until failure. Cross-section SEM images at $\Delta\varepsilon_{pl}/2 = 3.16 \times 10^{-3}$ in 50 cycles (c) and after surface polishing (d), showing that the majority of TBs and GBs are very stable. LA denotes the cyclic loading axis.

dislocation walls at very large γ_{pl} ($6 \times 10^{-5} < \gamma_{pl} < 7.5 \times 10^{-3}$). At very small γ_{pl}, it is maintained by dipole flip-flop in the veins and dislocation gliding back and forth in the irregular winding channels between the veins without dislocation multiplication and annihilation [50]. At very large γ_{pl}, there exists a dynamical equilibrium between the multiplication and annihilation of edge dislocations in the walls and high-density screw dislocations in the straight channels between the walls in the PSBs [50].

The grain size also has an important effect on the formation of the stable dislocation patterns of PSBs. In polycrystalline materials, the effect of constraints among adjacent grains becomes significant with decreasing grain size. The enhanced constraints tend to facilitate multiple rather than single slip behavior, even in grains with single-slip orientation, which inhibits PSB formation. Thus PSB formation becomes increasingly difficult with decreasing grain size. It has been shown that the critical grain size for stable PSB patterns formation is ~25 μm for CG-Cu [33,46]. This is consistent with the present result that ongoing cyclic hardening with no clear saturation stage occurs due to the multiple slip in CG-Cu (~9.8 μm), especially at large strain amplitudes, as seen in Fig. 2.

With grain size further decreasing into the submicrometer and nanometer regime, the corresponding severe deformed UFG/NG microstructure becomes rather unstable and undergoes marked cyclic softening at the early stage of fatigue [21–23,27–30]. Cyclic strain localizations, such as local grain coarsening and catastrophic shear bands, are largely responsible for the cyclic softening.

Hence, based on the above discussion, it is easy to find that both the stable dislocation patterns induced by single-slip systems (such as PSBs) and the relatively stable microstructure are probably two essential conditions for the cyclic stability of materials. Even though the average grain size of the present polycrystalline nt-Cu samples is a few micrometers (~4–6 μm), which is much smaller than the critical value observed for forming stable dislocation pattern in CG metals, the cyclic stability of nt-Cu, rather than the cyclic softening of UFG-Cu, is still observed under tension–compression fatigue tests. Next, the cyclic stability and cyclic mechanism of nt-Cu with highly oriented nanoscale twins will be discussed.

Fig. 5a and b reveals the typical plane and cross-section SEM observations of nt-Cu-B samples under tension–compression fatigue tests. Compared with the glossy surface in the as-deposited sample, two sets of roughly mutually perpendicular deformation features in a few grains are observed on the plane-viewed nt-Cu samples after being fatigued at the plastic strain amplitude of 5.6×10^{-4}, as shown in Fig. 5a. Most of the deformation features are principally concentrated at ~45° relative to the cyclic loading axis. These deformation features are parallel to each other in the single grain and distribute in the grain

interiors. Note that they do not transfer through GBs. The above evidence suggests that the slip band traces result from the dislocation activity with a single primary slip system, rather than the shear band (Fig. 5a). Subsequently, cross-sectional SEM observations show that many "zigzag" slip bands across a few TBs are detected in some grain interiors (Fig. 5b). The slip bands in single twin interiors are parallel to each other and mirror the slip bands in the adjacent matrix. These deformation features are analogous to those observed in nt-Cu under tension–tension stress-controlled fatigue tests [18], where dislocations with the slip plane inclined to TBs but the slip direction parallel to TBs are preferentially activated and dominate the plastic deformation.

In order to investigate the intrinsic fatigue mechanism, a nt-Cu-B specimen was selected and interrupted at 50 cycles when reaching the cyclic steady state at a plastic strain amplitude of 3.16×10^{-3}. Fig. 5c shows that "zigzag" slip bands across many TBs only appear in a few columnar grains, while the majority of columnar grains have no signs of plastic deformation. The slip steps are much more indistinct than that in Fig. 5b because they have undergone fewer cycles. After being polished, the GB morphologies of the fatigued nt-Cu are identical to that of the as-deposited sample, as seen in Fig. 5d. The absence of apparent deformation traces existing in twin interiors or at GBs suggests that both the nanotwin structures and the GBs in the present nt-Cu samples are very stable under tension–compression fatigue tests.

The above results thus suggest that the fatigue mechanism of nt-Cu samples under tension–compression fatigue tests is still dominated by single-slip threading dislocations slipping inside the twin interiors. The threading dislocations glide in the lamellar channels confined by neighboring TBs individually and bear close resemblance to hairpin threading dislocations observed in nanoscale thin films and multilayer materials [44,55]. The nanoscale twin confinement of threading dislocation motion in the twin/matrix layers determines the flow stress by the confined layer slip (CLS) model [18]. On the basis of the CLS model, the saturation resolved shear stress (τ_s) can be present as follows:

$$\tau_s = \frac{m\Delta\sigma}{2} = (34 \pm 16) + \frac{2028}{\lambda}\ln(0.625\lambda) \quad (2)$$

Generally, the saturation shear stress of nt-Cu is in proportion to $1/\lambda$, where λ is the twin thickness. This is consistent with the present results showing that the thinner the twin thickness, the higher the saturation stress reached. For example, based on the CLS model above, the saturation shear stresses of nt-Cu samples with λ of 75–110 nm is estimated to be 115–130 MPa. However, the shear stress can be as high as 175–190 MPa for nt-Cu samples with λ of 40–50 nm, as shown in Fig. 4.

Variations in the saturation stress of nt-Cu samples with the imposed plastic strain amplitude in Fig. 4 are most likely to be associated with threading dislocation glide in nanotwins with different thicknesses and in-plane orientations. For nt-Cu samples fatigued at a small plastic strain amplitude, the relative low saturation stress implies that dislocations are probably activated in twins with relative large twin spacing and the softest in-plane orientation. With increasing plastic strain amplitude, higher saturation stresses are required to accommodate the larger plastic strain by the activation of threading dislocations in smaller twins, even in some grains with hard orientations.

Besides the TB orientation parallel to the cyclic loading axis, both nanoscale twins and microsized grains also exhibit a crucial influence on the activation of a single primary slip system in nanotwin interiors. If the twin thickness is very large, i.e. in the micrometer regime, less restriction is applied on other slip systems by the twin planes. For example, secondary or multiple slips are often observed within twins in fatigued CG-Cu with annealing twins with large twin spacing [46–48]. However, for the nt-Cu samples in this study, only single slip of threading dislocations is preferentially activated, the secondary or multiple slip systems being severely suppressed by the tiny twin layers. Therefore, only the twin lamellae at the nanometer scale could be an effective barrier for stopping other dislocation activation. In addition, micrometer-sized grains also guarantee enough room for the threading dislocation to glide back and forth inside the nanotwin lamellar channels under tension–compression fatigue tests, rather than the detwinning phenomena in Ref. [16]. Thus the cyclic deformation of the nt-Cu sample is more like that in a fatigued "quasi-single" crystal material.

Guo et al. [56] systematically investigated the influence of the twin thickness on the dislocation configuration during cyclic deformation of polycrystalline Cu with a wide twin thickness distribution. They demonstrated that no dislocation patterns, such as PSBs or cell structures, could be formed when the twin thickness is less than 1 μm, similar to that observed in nanoscale metal films and multilayers (nanoscale laminated metal composites) [38,55]. Therefore, in spite of no PSB formation, single slip system activation of threading dislocations inside nanotwin lamellar channels and a relatively stable microstructure related to TBs and GBs are two key responsible factors for the steady state of nt-Cu samples under all strain amplitudes. More evidence of microstructure evolutions is needed to explain the underlying cyclic stability of nt-Cu samples fatigued under different strain amplitudes.

4.2. Grain size dependence of fatigue life in the LCF regime

In the LCF regime, strain-controlled fatigue life is primarily governed by the Coffin–Manson law [19,28], i.e.

$$\Delta\varepsilon_{pl}/2 = \varepsilon_f'(2N_f)^c \quad (3)$$

where ε_f' is the fatigue ductility coefficient, which is approximately equal to the fracture strain in the tensile test, and c is the fatigue ductility exponent, which ranges from -0.5 to -0.7 for most metal materials. According

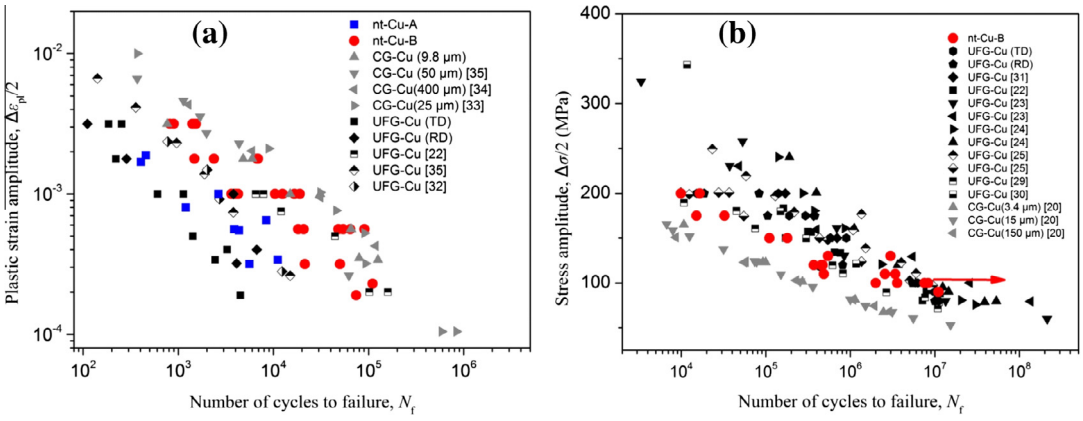

Fig. 6. Dependence of the fatigue life (N_f) on plastic strain amplitude ($\Delta\varepsilon_{pl}/2$–N) (a) and cyclic stress amplitude (S–N) (b) for nt-, CG- and UFG-Cu samples. Data for CG-Cu [20,33–35] and UFG-Cu [22–25,29–32,34,35] are also included for comparison. TD and RD denote that the cold-rolled UFG-Cu specimens are fatigued in the transverse direction and rolling direction, respectively. The purity of UFG-Cu (half-filled symbols) in the S–N curve is (99.9 wt.%) [25,29,30], whereas the others are 99.99 wt.% [22–24,31].

to the above Coffin–Manson equation, the fatigue life in the LCF regime is closely correlated with the ductility of the material. A good LCF performance requires a sufficiently high ductility [19,28].

For nt-Cu samples with high density of preferentially oriented nanoscale twins, the ductility is mainly dependent on the grain size, i.e. the length of twin lamellae. As investigated by tensile tests in Ref. [6], a considerable uniform strain is only achieved when the grain size is larger than the critical value, i.e. ~3 μm. With further increasing grain size, the ductility of nt-Cu samples increases monotonically.

In micrometer-length nanotwin channels, single-slip threading dislocations could glide conveniently to accommodate cyclic plastic strains, rather than strain localization occurring [27–29]. A larger grain size not only implies a larger amount of threading dislocations gliding back and forth inside lamellar nanotwin channels, but also guarantees that the threading dislocation can travel a relatively longer distance along the twin channels. The interactions between adjacent threading dislocations are very small with large sized grains. Based on the above analysis, nt-Cu samples with larger grain size can accommodate the larger cyclic plastic strain and have a longer fatigue life in the LCF regime. As seen in Fig. 6a, the strain-controlled fatigue life of nt-Cu is relatively enhanced over that of twin-free cold-rolled UFG-Cu. The fatigue life of nt-Cu-B samples with

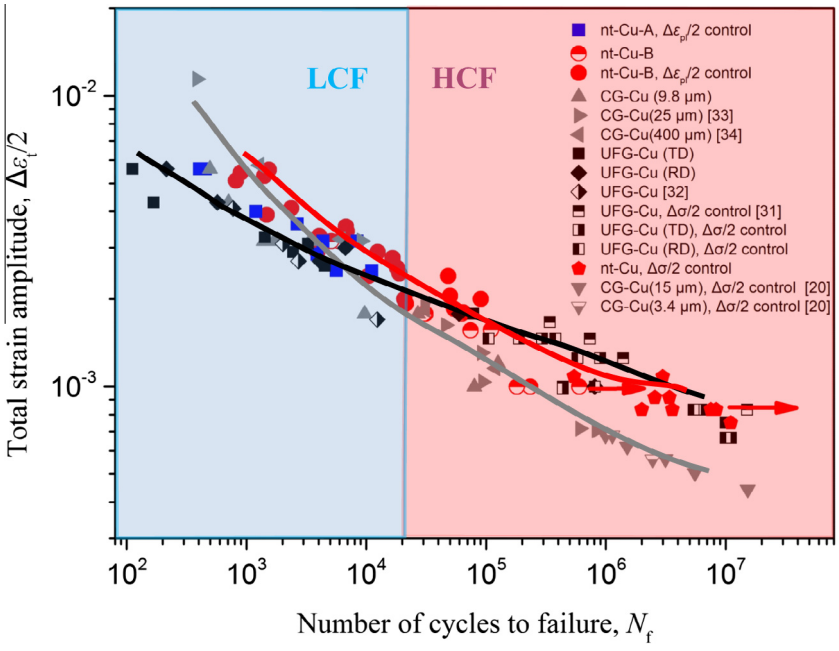

Fig. 7. Fatigue lives of nt-, CG- and UFG-Cu samples in a total strain amplitude–fatigue life diagram, showing that superior fatigue performances in both LCF and HCF regimes are achieved in nt-Cu samples. Data for CG-Cu [20,33,34] and UFG-Cu [31,32] are included for comparison. The data under plastic strain and stress control are denoted; others are obtained under total strain control.

a larger grain size is longer than that of nt-Cu-A and even comparable to that of the twin-free CG counterparts. The larger the grain size, the longer the low cycle fatigue life achieved.

Besides the LCF performance, the grain size also strongly influences the structural stability of nt-Cu sample. A main feature of the plastic deformation of columnar-grained nt-Cu is inhomogeneous during uniaxial tension: GB regimes usually take larger plastic strain than that sustained by grain interiors [6]. In the vicinity of GBs, the high density of dislocations gradually evolve into dislocation cells or subgrains as the strain increases and even detwinning induces elimination or thickening of growth twins [6]. Such GB-associated strain softening would be more serious in nt-Cu samples with small grain size and twin thickness, interpreting the fact that substantial volumes of nanotwins are destroyed and developed to the extended dislocation walls in fatigued nt-Cu samples with an average grain size of ~500 nm, as observed by Shute et al. [16].

In contrast, the grain sizes of both nt-Cu samples in the present study are about 10 times larger than that in Ref. [16], and the plastic deformation is more homogeneous in the grain interior and GBs, as shown in Fig. 5b. The GB-associated strain softening is suppressed by the larger grain size, and enhanced ductility and stability of microstructure are achieved. Therefore, both nanotwin structures and GBs in nt-Cu samples are still very stable, even when fatigued at very large plastic strain amplitude. However, the detailed dislocation morphologies associated with the intrinsic fatigue mechanism of nt-Cu samples still need to be further studied.

4.3. Enhanced low cycle and high cycle property synergy

The plastic strain–life ($\Delta\varepsilon_{pl}/2$–N) and stress–life (S–N) curves of all Cu samples with different microstructures in Fig. 6a and b reveal the HCF and LCF properties as a function of the fatigue life, N_f. As demonstrated in Section 4.2, nt-Cu samples have a superior fatigue life in the LCF regime under strain control, which benefits from their considerable ductility. Interestingly, the advantage for nt-Cu still exists in the HCF regime under stress control, as shown in Fig. 6b. In a fatigue life span of 10^4–10^6, the HCF property of nt-Cu is superior to that of CG-Cu. With increasing fatigue life, i.e. at 10^7 cycles, the fatigue limit (σ_{-1}) of nt-Cu-B is up to ~90 MPa, significantly higher than that of the CG-Cu (~50 MPa), and coincidentally resembles that of UFG Cu. In general, the stress-controlled fatigue life and endurance limit in the HCF regime are generally dominated by the strength, based on the Basquin law [19,28]. So, in stress-controlled HCF tests, nt-Cu samples with high strength following the CLS model still possess better fatigue life and a higher endurance limit than CG-Cu.

Fig. 7 summarizes the total strain–fatigue life diagrams for nt-, CG- and UFG-Cu samples in the present study and in the literature [20,31–34]. Under total strain amplitude control, the nt-Cu samples exhibit a constant plastic strain amplitude in the cyclic stability state, which is essentially distinct from the gradually increasing $\Delta\varepsilon_{pl}/2$ for UFG-Cu and decreasing $\Delta\varepsilon_{pl}/2$ for CG-Cu [19]. In order to distinguish the LCF and HCF regimes in this plot, a transition life is defined as the number of cycles to failure at which the elastic and plastic strain amplitudes are equal in nt-Cu samples, as defined in Ref. [19]. The experimental transition life is about 2×10^4 for the nt-Cu specimens. As seen in Fig. 7, the diagram can be divided into two regimes, the fatigue properties of the nt-Cu samples being superior to those of CG-Cu in both the LCF and HCF regimes. These results suggest that nanoscale twins in micrometer-sized grains enhance the synergy of both LCF and HCF fatigue properties of Cu appreciably, totally breaking down the trade-off of fatigue performance in the LCF and HCF regimes for the CG and UFG counterparts [22–24,27–30].

By introducing a high density of preferentially oriented nanotwins embedded within micrometer-sized grains, nt-Cu samples not only exhibit enhanced fatigue life in the LCF regime, but also sustain an extremely high fatigue limit in the HCF regime, which is fundamentally distinct from twin-free CG-Cu and UFG-Cu metals. The activation of single-slip threading dislocation glide in nanotwin channels results in a characteristic cyclic stability state, where the saturation stress depends on the twin thickness and low cycle fatigue life is closely correlated with the grain size. The present study not only provides detailed experimental data for the stress-controlled and strain-controlled fatigue tests of nt-Cu, but also provides insight into new possibilities for enhancing the fatigue performance of metals by tailoring the nanotwinned microstructures, such as with a larger grain size and a smaller twin thickness.

5. Conclusions

High-purity bulk Cu samples containing highly aligned nanoscale twins have been subjected to tension–compression strain-controlled fatigue. After a short, initially rapid cyclic hardening stage, the nt-Cu specimens reach a cyclic stability state with stable hysteresis loops. The effective confinement of threading dislocation inside nanoscale twin lamellar channels dominates the cyclic deformation and saturation behavior. During fatigue, the majority of TBs and GBs in most grains are quite stable. Both single-slip threading dislocation glide inside nanotwin lamellar channels and relatively stable microstructure are probably responsible for the cyclic stability of nt-Cu samples.

The higher saturation stress for nt-Cu samples is achieved at the larger imposed strain amplitude. Both twin thickness and grain size affect the fatigue properties of the nt-Cu specimens. The smaller twin thickness would benefit for a higher saturation stress, while the larger grain size is conducive to a longer fatigue life. For the present nt-Cu specimens with nanoscale twins and micrometer-sized columnar grains, a long fatigue life in the LCF regime and a high fatigue limit in the HCF regime are achieved

simultaneously, and these are fundamentally superior to the CG-Cu and UFG-Cu counterparts.

Acknowledgements

The authors acknowledge the National Basic Research Program of China (973 Program, 2012CB932202), financial support from the National Science Foundation of China (Grant Nos. 5131171 and 51471172), the Danish National Research Foundation and the National Natural Science Foundation of China (Grant No. 50911130230) for the Danish–Chinese Center for Nanometals. The authors are grateful to Profs. H. Mughrabi, H.J. Gao and Z.H. Jin for stimulating discussions, and Mr. S. Jin for nanotwinned Cu sample preparation.

References

[1] Christian JW, Mahajan S. Prog Mater Sci 1995;39:1.
[2] Lu K, Lu L, Suresh S. Science 2009;324:349.
[3] Lu L, Shen YF, Chen XH, Qian LH, Lu K. Science 2004;304:422.
[4] Shen YF, Lu L, Lu QH, Jin ZH, Lu K. Scr Mater 2005;52:989.
[5] Dao M, Lu L, Shen YF, Suresh S. Acta Mater 2006;54:5421.
[6] You ZS, Lu L, Lu K. Acta Mater 2011;59:6927.
[7] Zhang X, Wang H, Chen XH, Lu L, Lu K, Hoagland RG, et al. Appl Phys Lett 2006;88.
[8] Hodge AM, Wang YM, Barbee TW. Scr Mater 2008;59:163.
[9] Asaro RJ, Suresh S. Acta Mater 2005;53:3369.
[10] Zhu T, Li J, Samanta A, Kim HG, Suresh S. Proc Natl Acad Sci USA 2007;104:3031.
[11] Jin ZH, Gumbsch P, Albe K, Ma E, Lu K, Gleiter H, et al. Acta Mater 2008;56:1126.
[12] Shabib I, Miller RE. Acta Mater 2009;57:4364.
[13] Li XY, Wei YJ, Lu L, Lu K, Gao HJ. Nature 2010;464:877.
[14] Tang L, Lu L. Acta Metall Sin 2009;45:808.
[15] Shute CJ, Myers BD, Xie S, Barbee TW, Hodge AM, Weertman JR. Scr Mater 2009;60:1073.
[16] Shute CJ, Myers BD, Xie S, Li SY, Barbee Jr TW, Hodge AM, et al. Acta Mater 2011;59:4569.
[17] Singh A, Tang L, Dao M, Lu L, Suresh S. Acta Mater 2011;59:2437.
[18] Pan QS, Lu QH, Lu L. Acta Mater 2013;61:1383.
[19] Suresh S. Fatigue of materials. 2nd ed. Cambridge: Cambridge University Press; 1998.
[20] Thompson AW, Backofen WA. Acta Metall 1971;19:597.
[21] Meyers MA, Mishra A, Benson DJ. Prog Mater Sci 2006;51:427.
[22] Höppel HW, Brunnbauer M, Mughrabi H. In: Proceedings of materials week 2000. Frankfurt: Werkstoffwoche-Partnerschaft; 2000.
[23] Lukáš P, Kunz L, Svoboda M. Kovove Mater 2009;47:1.
[24] Goto M, Han SZ, Yakushiji T, Kim SS, Lim CY. Int J Fatigue 2008;30:1333.
[25] Zhang ZJ, An XH, Zhang P, Yang MX, Yang G, Wu SD, et al. Scr Mater 2013;68:389.
[26] Hanlon T, Kwon YN, Suresh S. Scr Mater 2003;49:675.
[27] Mughrabi H, Höppel HW, Kautz M. Scr Mater 2004;51:807.
[28] Mughrabi H, Höppel HW. Int J Fatigue 2010;32:1413.
[29] Agnew SR, Vinogradov AY, Hashimoto S, Weertman JR. J Electron Mater 1999;28:1038.
[30] Vinogradov A, Hashimoto S. Mater Trans JIM 2001;42:74.
[31] Ding HZ, Mughrabi H, Höppel HW. Fatigue Fract Eng Mater Struct 2002;25:975.
[32] Kwan CCF, Wang ZR. Proc Eng 2010;2:101.
[33] Mughrabi H, Wang R. In: Lukáš P, Polák J, editors. Basic mechanisms in fatigue of metals. Prague: Amsterdam: Academia/Elsevier; 1988.
[34] Korn M, Lapovok R, Bohner A, Höppel HW, Mughrabi H. Kovove Mater 2011;49:51.
[35] Wang QJ, Du ZZ, Liu XY, Kunz L. Mater Sci Forum 2011;682:231.
[36] Wang Y, Li J, Hamza AV, Barbee TW. Proc Natl Acad Sci USA 2007;104:11155.
[37] Broedling NC, Hartmaier A, Buehler MJ, Gao H. J Mech Phys Solids 2008;56:1086.
[38] Lesuer DR, Syn CK, Sherby OD, Wadsworth J, Lewandowski JJ, Hunt WH. Int Mater Rev 1996;41:169.
[39] Wang YC, Misra A, Hoagland RG. Scr Mater 2006;54:1593.
[40] Zhu XF, Zhang GPJ. Phys D Appl Phys 2009;42.
[41] Liu HS, Zhang B, Zhang GP. Scr Mater 2011;65:891.
[42] Mughrabi H. Mater Sci Eng 1978;33:207.
[43] Cheng AS, Laird C. Mater Sci Eng 1981;51:111.
[44] Misra A, Hirth JP, Hoagland RG. Acta Mater 2005;53:4817.
[45] Rasmussen KV, Pedersen OB. Acta Metall 1980;28:1467.
[46] Mughrabi H, Wang R. In: Hansen N, Horsewell A, Leffers T, Lilholt H, editors. Proceedings of the second Risø international symposium on metallurgy and material science. Denmark: Risø National Laboratory; 1981.
[47] Winter AT, Pedersen OR, Rasmussen KV. Acta Metall 1981;29:735.
[48] Polák J, Klesnil M. Mater Sci Eng 1984;63:189.
[49] Pedersen OB, Rasmussen KV, Winter AT. Acta Metall 1982;30:57.
[50] Mughrabi H, Ackermann F, Herz K. ASTM Spec Tech Pub 1979;675:68.
[51] Winter AT. Philos Mag 1974;30:719.
[52] Finney JM, Laird C. Philos Mag 1975;31:339.
[53] Basinski ZS, Basinski SJ. Prog Mater Sci 1992;36:89.
[54] Mughrabi H, Pschenitzka F. Philos Mag 2005;85:3029.
[55] Nix W. Metall Trans A 1989;20:2217.
[56] Guo XL, Lu L, Li SX. Acta Metall Sin 2005;41:23.